

Local image fitting-based active contour for vector-valued images

Akmal Shafiq Badarul Azam¹, Abdul Kadir Jumaat^{1,2}, Mohd Azdi Maasar³, Mohamed Faris Laham⁴, Normahirah Nek Abd Rahman⁵

¹School of Mathematical Sciences, College of Computing, Informatics and Mathematics, Universiti Teknologi MARA, Shah Alam, Malaysia

²Institute for Big Data Analytics and Artificial Intelligence (IBDAAI), Universiti Teknologi MARA, Shah Alam, Malaysia

³School of Mathematical Sciences, College of Computing, Informatics and Mathematics,

Universiti Teknologi MARA Negeri Sembilan Branch, Seremban, Malaysia

⁴Institute for Mathematical Research, Universiti Putra Malaysia, Serdang, Malaysia

⁵Pusat GENIUS@Pintar Negara, Universiti Kebangsaan Malaysia, Bangi, Malaysia

Article Info

Article history:

Received Mar 28, 2023

Revised Jul 7, 2023

Accepted Jul 16, 2023

Keywords:

Active contour

Intensity inhomogeneous image

Selective image segmentation

Variational level set

Vector-valued images

ABSTRACT

Variational active contour seeks to segment or extract desired object boundaries for further analysis. The model can be divided into global segmentation and selective segmentation. Selective segmentation, which focuses on segmenting a particular object, is preferable to the global model. Recently, a number of selective segmentation models have been developed to precisely extract an object on grayscale images. Nevertheless, if the input image is vector-valued (colour), these models merely convert it to a grayscale image, resulting in data loss owing to the reduction in image dimension. Furthermore, they may have poor segmentation performance due to the intensity inhomogeneous images. Therefore, a new model on variational selective active contour for segmenting vector-valued images has been proposed that incorporates the concepts of local image fitting and distance-based fitting terms into a variational minimization energy functional. Moreover, a Gaussian function was used as a regularizer to replace the computationally expensive Total Variation term. Then, the proposed model's Euler Lagrange equation has been provided to solve the model. When segmenting an object in inhomogeneous intensity images, the result of the proposed model was about 30% more accurate based on the Jaccard value and about 3 times faster than other existing methods.

This is an open access article under the [CC BY-SA](https://creativecommons.org/licenses/by-sa/4.0/) license.



Corresponding Author:

Abdul Kadir Jumaat

School of Mathematical Sciences, College of Computing, Informatics and Mathematics

Institute for Big Data Analytics and Artificial Intelligence (IBDAAI), Universiti Teknologi MARA

Kompleks Al-Khawarizmi, 40450 Shah Alam, Selangor, Malaysia

Email: abdulkadir@tmsk.uitm.edu.my

1. INTRODUCTION

Image segmentation is one of the most complex and vital mathematical problems in image processing that is beneficial in many applications such as medical image analysis, biometric identification, object detection and classification [1]-[7]. Several segmentation approaches that have been established including learning-based approaches (machine and deep learning) and active contour method (ACM). The learning-based approaches although effective however required a huge amount of data which is not always available. For small amounts of data, they are less accurate. On the other hand, the ACM which is independent of amount of data is a variational mathematical model that has been ascertained as the most successful segmentation approach. Two

types of ACM exist: global segmentation and selective segmentation. Global segmentation requires the segmentation of the boundaries of all objects within an image. In contrast, selective segmentation extracts only the required object according to predetermined geometric constraints from an input image [2]-[3].

The C-V model by Chan and Vese [8] is the most widely used region-based global ACM. However, this C-V model is only applicable to grayscale images. This led Chan *et al.* [9] to propose the chan-sandberg-vese (CSV) model, a vector-valued image segmentation model based on active contours that able to produce better results as more information is included. Despite this, the use of global image information in both C-V and CSV models makes them difficult to segment intensity inhomogeneous images. Intensity inhomogeneity refers to the presence of smooth variations in intensity across different regions of an image [10], arises due to the data acquisition process and external factors such as imperfection in the camera, inconsistencies in ambient daylight and artificial lighting. This problem poses difficulties during the image segmentation process, especially using an ACM that depends on the intensity homogeneity of the desired object in an image. In order to encounter the intensity inhomogeneity problem, Zhang *et al.* [11] proposed a new model namely the local image fitting (LIF) approach, which relies on the disparities between the original and the local fitting images in order to extract the local image information from a grayscale image. In addition, they also introduced a Gaussian function for variational level set regularization to speed up the processing time. Since then, many researchers have used the LIF and Gaussian function as the regularizer in segmenting intensity inhomogeneous images [12]-[16].

All the approaches described above are immensely useful for tasks requiring the segmentation of all features in a single image. Thus, they are inapplicable in the case of selective segmentation. This study is concerned with the selective segmentation type to segment vector-valued or colour images. The integration of this method with medical imaging disciplines [17]-[18], biometric authentication [19] and text processing [20] has its own significant potential. Nguyen *et al.* [21] introduced a robust interactive selective image segmentation model for vector-valued images that is state-of-the-art. We referred to this model as interactive image segmentation (IIS). Among other authors, this IIS model uses two geometric constraints to selectively segment the desired objects in an input image (foreground and background strokes). The implementation results have proven that their model was superior to other interactive state-of-the-art segmentation models that were stated in the paper. However, the model may give unsatisfactory result in segmenting fine shape.

Recently, another selective type of variational ACM termed distance selective segmentation 2 (DSS2) model was proposed by Ghani and Jumaat [22]. A distance function with only a single geometrical constraint was used in the formulation of the DSS2 model with promising results for colour or vector-valued images. However, the DSS2 model has a high computational cost because of the existence of total variation (TV) term in the formulation. In addition, the DSS2 model is not designed to segment a targeted object in vector-valued images having intensity inhomogeneity.

Thus, this paper aims to develop a new model on variational selective active contour to segment vector-valued images with intensity inhomogeneity efficiently. The subsequent section of this study provides the methodology where it describes the suggested model's formulation and its solution by considering the local image fitting energy and distance function with Gaussian regularizer in the new models's formulation. Following that, the experimental results and discussion are provided in section 3 before concluding in section 4.

2. METHOD

The idea of formulating the new model is achieved by integrating the LIF model [11] and distance function of DSS2 model [22] into a variational minimization energy functional. Furthermore, a Gaussian function is proposed as a regularizer to replace the computationally expensive TV term. The methodology of the proposed model will be explained based on the flow chart in Figure 1.

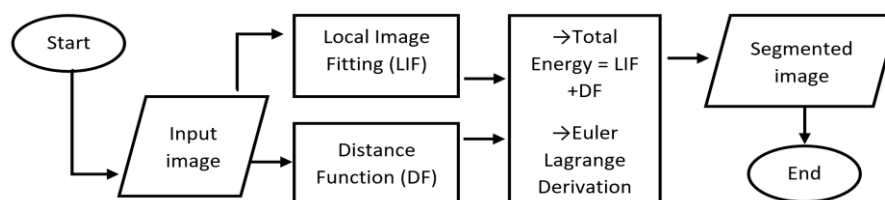


Figure 1. Methodology of the proposed model

Based on Figure 1, the LIF energy and distance function (DF) fitting term of an input image are computed. After that, a total energy minimization functional that represents the new model is formulated to segment the input image by integrating the LIF and DF energies. Next, the Euler Lagrange equation is derived from the total energy minimization functional to obtain the segmented output image. In the next subsection, each step is explained in detail.

2.1. Input image

This research involves the segmentation of test images which consist of a combination of synthetic, natural and medical images obtained from various image database in [23]-[29]. Their groundtruths which contained the segmented regions were obtained from the same database. The test images were vector-valued images with intensity inhomogeneity to test the ability of the proposed model.

2.2. Local image fitting

Zhang *et al.* [11] invented LIF model to effectively segmenting image with intensity inhomogeneity. Assume that for an image $u = u(x, y)$ in a domain Ω , the regularized local image fitting energy function in the level set formulation E_ϵ^{LIF} is defined as follows:

$$E_\epsilon^{LIF}(\phi) = \frac{1}{2} \int_\Omega \left| u - \left(n_1 H_\epsilon(\phi) + n_2 (1 - H_\epsilon(\phi)) \right) \right|^2 dx dy \tag{1}$$

where $H_\epsilon(\phi)$ represents the Heaviside function such that $H_\epsilon(\phi) = 0.5(1 + (2/\pi) \arctan(\phi/\epsilon))$ while n_1 and n_2 are the averages intensity of the interior and exterior in a local region. In this research, we extend the formulation in (1) into vector-valued framework to process colour images. Thus, the (1) can be transformed into the following new (2).

$$E_\epsilon^{LIF}(\phi) = \frac{1}{2} \int_\Omega \frac{1}{N} \sum_{i=1}^N \left[u^i - \left(n_1^i H_\epsilon(\phi) + n_2^i (1 - H_\epsilon(\phi)) \right) \right]^2 dx dy \tag{2}$$

Here, $u^i = u^i(x, y)$ is the i^{th} channel of a colour image on Ω with $i = 1, 2, \dots, N$ channels. For the vector valued (colour) image, the value of N is three. The functions $n_1^i = (n_1^1, \dots, n_1^N)$ and $n_2^i = (n_2^1, \dots, n_2^N)$ are the intensity averages of interior and exterior in a local region that could be expressed in the following way:

$$\begin{aligned} n_1^i(\phi) &= \text{mean} \left(u^i \in (\{(x, y) \in \Omega | \phi(x, y) > 0\} \cap K_\sigma(x, y)) \right) \\ n_2^i(\phi) &= \text{mean} \left(u^i \in (\{(x, y) \in \Omega | \phi(x, y) < 0\} \cap K_\sigma(x, y)) \right) \end{aligned} \tag{3}$$

here, a truncated Gaussian window $K_\sigma(x, y) = e^{-(x^2+y^2)/2\sigma^2}$ is used with a standard deviation σ and a size of $(4\omega + 1) \times (4\omega + 1)$, where ω is the greatest integer smaller than σ . Thus, in (3) which contains local image information is vital to segment intensity inhomogeneous images, where the global image information will ignore the small or local features of an image [30].

2.3. Distance function

The distance selective segmentation 2 (DDS2) model is a selective type of variational ACM for vector-valued images that was proposed by Ghani and Jumaat [22]. The DSS2 model integrated the idea of the distance function as a fitting term with the formulation of the CSV model [9]. Assume that on an image $u = u(x, y)$, there are m_1 geometrical points that must be near to the desired object boundary and form a marker set B to be inputted by the user as follows:

$$B = \{w_j = (x_j^*, y_j^*) \in \Omega, 1 \leq j \leq m_1\} \subset \Omega \tag{4}$$

where $m_1 \geq 3$ will connect the markers and construct an initial polygon G that drives its evolution towards a curve Γ . Then, the distance function $F_d(x, y)$ of point $(x, y) \in \Omega$ from $(x_g, y_g) \in G$ that can assist in capturing a targeted object in the segmentation process is given as (5).

$$F_d(x, y) = \sqrt{(x - x_g)^2 + (y - y_g)^2} = \min_{g \in G} \left\| (x, y) - (x_g, y_g) \right\| \tag{5}$$

2.4. Total energy functional and euler lagrange equation

This study aims to develop a model that can selectively segment the vector-valued images having inhomogeneous intensity. As a result, we proposed a new selective segmentation model called the selective

local image fitting (SLIF) model. To achieve this, we incorporated the idea of the distance fitting term of the DSS2 model with the local image fitting energy of the LIF model into a variational energy functional in a vector-valued framework. Thus, the following (6) in level set framework [31]-[33] defined the SLIF model (6).

$$\min_{\phi} \left\{ E_{\varepsilon}^{SLIF}(\phi) = \frac{1}{2} \int_{\Omega} \frac{1}{N} \sum_{i=1}^N \left(u^i - n_1^i H_{\varepsilon}(\phi) - n_2^i (1 - H_{\varepsilon}(\phi)) \right)^2 dx dy + \int_{\Omega} \theta H_{\varepsilon}(\phi) F_d(x, y) dx dy \right\} \quad (6)$$

Here, the segmentation curve $\Gamma = \{(x, y) \in \Omega | \phi(x, y) = 0\}$ and $u^i = u^i(x, y)$ is the i^{th} channel of an original image on Ω with $i = 1, 2, \dots, N$ channels. In this research, the value of N is three which represents the vector valued (RGB) image. To solve the proposed model, the Euler Lagrange equation is derived defined as follows:

$$-\delta_{\varepsilon}(\phi) \left[\frac{1}{N} \sum_{i=1}^N \left(u^i - n_1^i H_{\varepsilon}(\phi) - n_2^i (1 - H_{\varepsilon}(\phi)) \right) (n_1^i - n_2^i) - \theta F_d \right] = 0 \quad (7)$$

the popular gradient descent method [34]-[36] is used to solve (7) numerically. Then, we obtain the following gradient descent flow:

$$\frac{\partial \phi}{\partial t} = -\frac{\partial E_{\varepsilon}^{SLIF}}{\partial \phi} = \delta_{\varepsilon}(\phi) \left[\frac{1}{N} \sum_{i=1}^N \left(u^i - n_1^i H_{\varepsilon}(\phi) - n_2^i (1 - H_{\varepsilon}(\phi)) \right) (n_1^i - n_2^i) - \theta F_d \right] \quad (8)$$

to ensure smoothness of segmentation curve, we convolve the result from (8) with a Gaussian function $G_{\zeta} = e^{-(x^2+y^2)/2\zeta^2}$, with standard deviation ζ . This technique is less computational expensive than the traditional TV term.

2.5. Algorithm to implement the SLIF model

In this study, MATLAB R2018a was used to run the experiments. The central processing unit (CPU) processor used was an Intel Core i5-8250U CPU running at 1.60 GHz with 8GB of installed memory (RAM). Two stopping criteria were used to stop the program automatically: a tolerance value $tol = 0.005$ and the maximum number of iterations, $maxit = 3000$. The implementation process for our SLIF model is depicted in the following Algorithm 1.

Algorithm 1. Algorithm for SLIF model

1. Set the value of parameters θ, σ , and ε .
2. Define the marker set \mathcal{C} and determine $F_d(x, y)$ using Equation (5).
3. Initialize ϕ^0 (when $m=0$) such that Γ is the boundary of G .
4. Compute $n_1^i(\phi^m)$ and $n_2^i(\phi^m)$ using equation (3).
5. Evolve ϕ based on equation (8) to get ϕ^{m+1} .
6. Regularize ϕ by convolving ϕ^{m+1} with a Gaussian function G_{ζ} .
7. If $\frac{\|\phi^{m+1} - \phi^m\|}{\|\phi^m\|} \leq tol$ or maximum number of iteration ($maxit$) reached 3000, then stop the program. Otherwise, return to step 4.

3. RESULTS AND DISCUSSION

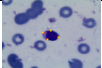





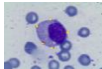

















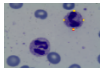





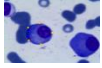





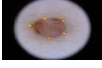





Three experiments were carried out. Firstly, we compared our proposed model, namely the SLIF model, with the DSS2 model by Ghani and Jumaat [22] in terms of segmentation accuracy and efficiency. Then, we are interested in comparing the accuracy of segmentation of our SLIF model with the IIS model by [21], which is considered a cutting-edge selective segmentation model for segmenting vector-valued images. Lastly, we performed the parameter sensitivity analysis on our SLIF model.

The accuracy of our proposed model was evaluated by visual observation as well as by dice similarity coefficient (DSC) and jaccard similarity coefficient (JSC). The DSC and JSC values are graded on a scale from 0 to 1, with 0 indicating that there is no overlap between the two data sets and 1 indicating that there is a complete congruence [37]. Meanwhile, the efficiency of the SLIF model was determined by utilizing the tic and toc built-in functions in MATLAB to measure the time processing for both models. We repeated the experiments three times and the average time processing \bar{t} was determined to guarantee the consistency of the results. We set the parameters $\varepsilon = 1$, $\zeta = 0.45$, $\theta = [5, 1500]$, $\sigma = [5, 25]$, the mask of the Gaussian function is 5×5 , the size of test images is 128×128 pixels, the maximum iteration to 3000 and the value of tolerance tol to 0.005.

3.1. Experiment 1: Comparison of the SLIF model with the DSS2 model

In this Experiment 1, we were compared the performance of the proposed SLIF model with the existing DSS2 model. There were 14 test images used in this experiment. The test images with markers and the associated results generated by the DSS2 model and the proposed SLIF model are shown in Table 1.

Table 1. Segmentation results between the SLIF and DSS2 models

Test image	SLIF model	DSS2 model	Test image	SLIF model	DSS2 model
					
1a	1b	1c	8a	8b	8c
					
2a	2b	2c	9a	9b	9c
					
3a	3b	3c	10a	10b	10c
					
4a	4b	4c	11a	11b	11c
					
5a	5b	5c	12a	12b	12c
					
6a	6b	6c	13a	13b	13c
					
7a	7b	7c	14a	14b	14c

Based on Table 1, the images in the first and fourth column were test images with initial yellow markers to indicate the selected object that needs to be segmented. They were medical test images in Table 1(1a-8a), natural test images in Table 1(9a-10a) and synthetic test images in Table 1(11a-14a). The images in the second column of Table 1 (1b-7b) and fifth column of Table 1(8b-14b) were the segmentation results for the SLIF model in binary form. The segmentation output for DSS2 model were displayed in the third column of Table 1(1c-7c) and the last column of Table 1(8c-14c).

By visual observation, all the targeted objects could be segmented well by our SLIF model indicated in Table 1(1b-14b) compared to the DSS2 model which are indicated in Table 1(1c-14c). The DSS2 model unable to capture some important features especially for test images in Table 1(11a-14a) where the respective segmented results of the DSS2 model as shown in Table 1(11c-14c) are incomplete. This is not the case for the proposed SLIF model where it capable to capture the shapes of the targeted objects successfully as indicated in Table 1(11b-14b).

Even though the DSS2 model has a constraint distance function defined in the formulation to capture only the targeted object, there is no local intensity information contained in the DSS2 model, which is vital for the segmentation of images with inhomogeneous intensities. The optimum intensity constants in the DSS2 formulation that approximates the global average of inner and outer intensities of the contour Γ could be very different from the original image u^i if the intensities within the internal and exterior of the contour Γ are not homogeneous. As a result, the DSS2 model cannot segment intensity inhomogeneous vector-valued images.

For our SLIF model, the extraction of intensity information from the local region was used to govern the motion of the contour Γ and keep it within the borders of the targeted object. The local averages n_1^i and n_2^i in the SLIF formulation locally approximated the average inner and outer intensities of the contour Γ in a Gaussian window, which is more effective than the global averages intensity constants used in the DSS2 model to cope with inhomogeneous intensity images. In addition to visual observation, the average of segmentation accuracy and efficiency between the SLIF and DSS2 models were provided as well as shown in Table 2.

Table 2. Comparison of average accuracy and efficiency between the SLIF and DSS2 models

SLIF Model				DSS2 Model			
DSC	JSC	$\bar{\tau}$	Iteration	DSC	JSC	$\bar{\tau}$	Iteration
0.94	0.90	3.07	94	0.81	0.69	9.68	201





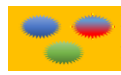

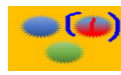

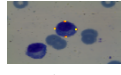

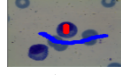











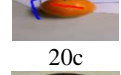


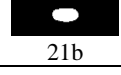

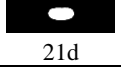
Based on Table 2, we can see that the average DSC and JSC values for our SLIF model were 0.94 and 0.90, respectively, which were about 16% and 30% higher than the DSS2 model respectively. Additionally, the SLIF model only required about 3.07 seconds to converge, which was about three times faster than the DSS2 model. Our SLIF model also only needs a small number of iterations to converge than the DSS2 model.

The DSS2 model has a TV term, which is difficult to solve numerically. However, our SLIF model utilized a Gaussian function to replace the traditional TV term in the level set regularization which makes the segmentation process faster. Overall, we may conclude that our SLIF outperformed the DSS2 model in terms of accuracy and efficiency in segmenting the region of interest (ROI) on the test images with intensity inhomogeneity.

3.2. Experiment 2: Comparison of the SLIF model with the IIS model

In this Experiment 2, we were interested in investigating the accuracy of our SLIF model by comparing it with one of the state-of-the-art models, which was the IIS model by Nguyen *et al.* [21]. There were seven test images used in this experiment. The test images with markers and the correlated results generated by the IIS model and the proposed SLIF model are shown in Table 3.

Table 3. Segmentation results between the SLIF and IIS models

Test image with markers	SLIF model	Test image with markers	IIS model
 15a	 15b	 15c	 15d
 16a	 16b	 16c	 16d
 17a	 17b	 17c	 17d
 18a	 18b	 18c	 18d
 19a	 19b	 19c	 19d
 20a	 20b	 20c	 20d
 21a	 21b	 21c	 21d

Based on Table 3, the test images were synthetic images as shown in Table 3(15a-16a), medical images in Table 3(17a-18a) and natural images in Table 3(19a-21a). The yellow marker sets used by the proposed SLIF model were indicated in the first columns of Table 3(15a-21a) while the third column of Table 3(15c-21c) indicated the IIS model's foreground (red) and background (blue) labels regions with two types of markers, which are different from a marker set used in our SLIF model. To keep the comparison fair, we place both models' foreground markers inside or relatively close to the targeted object, while the IIS model's background marker is placed outside the targeted object. The generated results for the SLIF model were demonstrated in the second column of Table 3(15b-21b) while the results delivered by the IIS model were displayed in the last column of Table 3(15d-21d).

Visual inspection shows that the IIS model performs just as well as our SLIF model in almost all problems. We recognize that the IIS model produces promising results when segmenting objects with intensity inhomogeneity. Nonetheless, there are a few circumstances where the IIS model could not segment appropriately where we found that the IIS model could not segment the jagged part of the targeted object for test images 16a and 19a clearly and concisely. The main reason is because the model is a hard segmentation which assumes the object to be segmented is smooth. Therefore, the IIS model cannot cleanly segment the targeted object with sophisticated shapes. In our SLIF model, the inclusion of the constructed polygon's Euclidean distance in the SLIF formulation is meant to confine the solution by enclosing values associated with a polygon region generated by the initial markers within the targeted object. As a result, the SLIF model outperforms the IIS model for test images 16a and 19a. The average segmentation accuracy between the SLIF and IIS models on the tested images is tabulated in Table 4.

Table 4 shows that the SLIF model's average DSC and JSC values were slightly higher than the IIS model. As a result, we can conclude that the segmentation accuracy of our SLIF model is comparable to that of the IIS model. We clarify that the interactive software provided by Nguyen *et al.* [21] lacks a time recording tool for implementing their IIS model. Thus, the time processing comparisons with our proposed models are not possible.

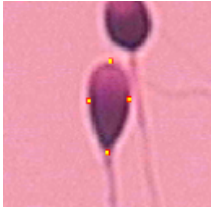



Table 4. Comparison of accuracy between the SLIF and IIS models

SLIF Model		IIS Model	
DSC	JSC	DSC	JSC
0.96	0.92	0.95	0.90

3.3. Experiment 3: Parameter sensitivity analysis

In this Experiment 3, we shall test the parameter sensitivity for our SLIF model. We focus on the area parameter θ which is the most important parameter that influence the segmentation result significantly. The main limitation of our proposed SLIF model is that this parameter must be manually tuned through trial and error in order to obtain meaningful and effective segmentation results. Table 5 illustrates the segmentation results of a test image with different parameters θ .

Table 5. Segmentation results with different values of parameter θ using the SLIF model

Test Image with Markers	Parameter Setting	Segmentation Result
	$\theta = 1$	
	$\theta = 200$	
	$\theta = 2000$	

The test image with markers located at the targeted region which is only the head of the large sperm was displayed in the first column of Table 5. In the second column, the values of θ were varied to test the effect on the segmentation results generated by the proposed SLIF model where we test with three values of $\theta = 1, 200$ and 2000 . The respected segmentation results were demonstrated in the last column of Table 5. As shown in Table 5, the segmentation result would be over-segmented if the parameter θ was too small ($\theta = 1$). As we can see, the tail of the targeted sperm and other nearby objects were segmented too. Meanwhile, the segmentation result could be just an undesirable polygon if the parameter θ was too large ($\theta = 2000$). The successful segmentation result was obtained if the parameter $\theta = 200$. Thus, to achieve an accurate segmentation result, the parameter must be determined by trial and error.

4. CONCLUSION

The primary purpose of this research is to segment a targeted object selectively in vector-valued images with intensity inhomogeneity using a variational active contour approach. As a result, we developed a new model called the SLIF model, which is formulated by incorporating the idea of the distance fitting term, local image fitting energy and Gaussian regularization term into a variational energy functional. In addition, we provided the proposed active contour model's Euler Lagrange equation to solve the SLIF model. Numerical experimentations demonstrated that the proposed SLIF model successfully segmented the object of interest in vector-valued images with better segmentation results compared to the existing models. The limitation of our proposed SLIF model is that the area parameter θ must be manually modified through trial and error to achieve significant and effective segmentation results. In the future, we will extend the work on formulating a convex 3-dimensional active contour model for both grayscale and vector-valued digital images.

ACKNOWLEDGEMENTS

The APC was funded by Pembiayaan Yuran Penerbitan Artikel (PYPA), Tabung Dana Kecemerlangan Pendidikan (DKP), Universiti Teknologi MARA (UiTM), Malaysia.




REFERENCES

- [1] A. K. Jumaat and K. Chen, "Three-dimensional convex and selective variational image segmentation model," *Malaysian Journal of Mathematical Sciences*, vol. 14, no. 3, pp. 437–450, 2020.
- [2] A. K. Jumaat and K. Chen, "A reformulated convex and selective variational image segmentation model and its fast multilevel algorithm," *Numerical Mathematics Theory Methods and Applications*, vol. 12, no. 2, pp. 403–437, 2019.
- [3] A. K. Jumaat and K. Chen, "An optimization-based multilevel algorithm for variational image segmentation models," *Electronic Transactions on Numerical Analysis*, vol. 46, pp. 474–504, 2017.
- [4] A. K. Jumaat et al., "Performance comparison of canny and sobel edge detectors on balloon snake in segmenting masses," in *2014 International Conference on Computer and Information Sciences (ICCOINS)*, 2014, pp. 1–5, doi: 10.1109/ICCOINS.2014.6868368.
- [5] S. S. Yasiran et al., "Microcalcifications segmentation using three edge detection techniques," in *International Conference on Electronic Devices, Systems and Applications*, pp. 207–211, 2012, doi: 10.1109/ICEDSA.2012.6507798.
- [6] A. K. Jumaat, W. E. Z. W. A. Rahman, A. Ibrahim, and R. Mahmud, "Segmentation and characterization of masses in breast ultrasound images using active contour," in *2011 IEEE International Conference on Signal and Image Processing Applications (ICSIPA)*, 2011, pp. 404–409, doi: 10.1109/ICSIPA.2011.6144126.
- [7] S. S. Yasiran et al., "Comparison between GVF snake and ED snake in segmenting microcalcifications," in *2022 7th International Conference on Image and Signal Processing and their Applications (ISPA)*, pp. 597–601, 2011, doi: 10.1109/ICCAIE.2011.6162204.
- [8] T. F. Chan and L. A. Vese, "Active contours without edges," *IEEE Transactions on Image Processing*, vol. 10, pp. 266–277, 2001, doi: 10.1109/83.902291
- [9] T. F. Chan, B. F. Sandberg, and L. A. Vese, "Active contours without edges for vector-valued images," *Journal of Visual Communication and Image Representation*, vol. 11, no. 2, pp. 130–141, 2000, doi: 10.1006/jvci.1999.0442
- [10] S. Soomro, A. Munir, and K.N. Choi, "Fuzzy c-means clustering based active contour model driven by edge scaled region information," *Expert Systems with Applications*, vol. 120, pp. 387–396, 2019, doi:10.1016/j.eswa.2018.10.052.
- [11] K. Zhang, H. Song, and L. Zhang, "Active contours driven by local image fitting energy," *Pattern Recognit.*, vol. 43, pp. 1199–1206, 2010, doi:10.1016/j.patcog.2009.10.010.
- [12] Y. Yang, W. Jia, and B. Wu, "Simultaneous segmentation and correction model for color medical and natural images with intensity inhomogeneity," *The Visual Computer*, vol. 36, pp. 717–731, 2020, doi: 10.1007/s00371-019-01651-4
- [13] E. Iqbal et al., "Saliency-driven active contour model for image segmentation," *IEEE Access*, vol. 8, pp. 208978–208991, 2020, doi: 10.1109/ACCESS.2020.3038945
- [14] S. Biswas and R. Hazra, "A level set model by regularizing local fitting energy and penalty energy term for image segmentation," *Signal Processing*, vol. 183, p. 108043, 2021, doi: 10.1016/j.sigpro.2021.108043.
- [15] J. Fang, H. Liu, J. Liu, H. Zhou, L. Zhang, and H. Liu, "Fuzzy region-based active contour driven by global and local fitting energy for image segmentation," *Applied Soft Computing*, vol. 100, 106982, 2021, doi: 10.1016/j.asoc.2020.106982.
- [16] S. Soomro, A. Munir, and K. N. Choi, "Fuzzy c-means clustering based active contour model driven by edge scaled region information," *Expert Systems with Applications*, vol. 120, pp. 387–396, 2019, doi:10.1016/j.eswa.2018.10.052.
- [17] N. F. Idris, M. A. Ismail, M. S. Mohamad, S. Kasim, Z. Zakaria, and T. Sutikno, "Breast cancer disease classification using fuzzy ID3 algorithm based on association function," *IAES International Journal of Artificial Intelligence (IJ-AI)*, vol. 11, no. 2, pp. 448, 2022, doi: 10.11591/ijai.v11.i2.pp448-461.
- [18] H. M. Ahmed and M. Y. Kashmola, "A proposed architecture for convolutional neural networks to detect skin cancers," *IAES International Journal of Artificial Intelligence (IJ-AI)*, vol. 11, no. 2, pp. 485, 2022, doi: 10.11591/ijai.v11.i2.
- [19] A. H. T. Al-Ghraiiri, A. A. Mohammed, and E. Z. Sameen, "Face detection and recognition with 180 degree rotation based on principal component analysis algorithm," *IAES International Journal of Artificial Intelligence*, vol. 11, no. 2, pp. 593–602, 2022, doi: 10.11591/ijai.v11.i2.pp593-602.
- [20] M. Z. Ansari, T. Ahmad, M. M. S. Beg, and N. Bari, "Language lexicons for Hindi-English multilingual text processing," *IAES International Journal of Artificial Intelligence (IJ-AI)*, vol. 11, no. 2, pp. 641, 2022, doi: 10.11591/ijai.v11.i2.pp641-648.
- [21] T. N. A. Nguyen, J. Cai, J. Zhang, and J. Zheng, "Robust interactive image segmentation using convex active contours," *IEEE Trans Image Process*, vol. 21, no. 8, pp. 3734–3743, 2012, doi: 10.1109/TIP.2012.2191566.
- [22] N. A. S. M. Ghani and A. K. Jumaat, "Selective segmentation model for vector-valued images," *Journal of Information and Communication Technology*, vol. 21, no. 2, pp. 149–173, 2022, doi: 10.32890/jict2022.21.2.1.
- [23] H. O. Ilhan, G. Serbes, and N. Aydin, "Automated sperm morphology analysis approach using a directional masking technique," *Computers in Biology and Medicine*, vol. 122, 103845, 2020, doi: 10.1016/j.compbiomed.2020.103845.
- [24] Ismahan. "Microscopic bone marrow images dataset." Available online: <https://www.kaggle.com/datasets/fanouna/microscopic-bone-marrow-images> (accessed on 27 November 2022).
- [25] N. C. F. Codella et al., "Skin lesion analysis toward melanoma detection: A challenge," in *Int. symposium biomedical imaging (ISBI), hosted by the International Skin Imaging Collaboration (ISIC)*, 2018, doi: 10.1109/isbi.2018.8363547
- [26] M. Y. Chen et al., "Automatic chinese food identification and quantity estimation," in *SA'12: SIGGRAPH Asia*, 2012, doi: 10.1145/2407746.2407775.
- [27] J. Li, C. Xia, and X. Chen, "A benchmark dataset and saliency-guided stacked autoencoders for video-based salient object detection," *IEEE Transactions on Image Processing*, vol. 27, pp. 349–364, 2018, doi: 10.1109/TIP.2017.2762594.
- [28] D. Martin, C. Fowlkes, D. Tal, and J. Malik, "A database of human segmented natural images and its application to evaluating segmentation algorithms and measuring ecological statistics," in *Proceedings Eighth IEEE International Conference on Computer Vision. ICCV 2001*, vol. 2, 2001, pp. 416–423, doi: 10.1109/ICCV.2001.937655.
- [29] S. Lankton and A. Tannenbaum, "Localizing region-based active contours," *IEEE Transactions on Image Processing*, vol. 17, pp. 2029–2039, 2008, doi: 10.1109/TIP.2008.2004611.
- [30] L. Mabood et al., "Multi-scale-average-filter-assisted level set segmentation model with local region restoration achievements," *Scientific Reports*, vol. 12, 15949, 2022, doi: 10.1038/s41598-022-19893-z
- [31] H. Ali, L. Rada, and N. Badshah, "Image segmentation for intensity inhomogeneity in presence of high noise," *IEEE Transactions on Image Processing*, vol. 27, pp. 3729–3738, 2018, doi: 10.1109/TIP.2018.2825101.
- [32] Z. Shahvaran, K. Kazemi and M. S. Helfroush, "Simultaneous vector-valued image segmentation and intensity nonuniformity correction using variational level set combined with Markov random field modeling," *Signal, Image and Video Processing*, vol. 10, pp. 887–893, 2016, doi: 10.1007/s11760-015-0836-7.
- [33] N. Badshah, F. Ullah, and Matiullah, "On segmentation model for vector valued images and fast iterative solvers," *Advances in Difference Equations*, vol. 221, pp. 1–16, 2018, doi: 10.1186/s13662-018-1669-9.




- [34] Y. Chen, P. Ge, G. Wang, G. Weng, and H. Chen, "An overview of intelligent image segmentation using active contour models," *Intelligence and Robotics*, vol. 3, pp. 23-55, 2023, doi: 10.20517/ir.2023.02.
- [35] Y. Kim, D. Kang, Y. Mok, S. Kwon and J. Paik, "A review on few-shot learning for medical image segmentation," *2023 International Conference on Electronics, Information, and Communication (ICEIC)*, Singapore, 2023, pp. 1-3, doi: 10.1109/ICEIC57457.2023.10049899.
- [36] J. H. Gagan, H. S. Shirsat, Y. S. Kamath, N. I. R. Kuzhuppilly, and J. R. H. Kumar, "Automated optic disc segmentation using basis splines-based active contour," in *IEEE Access*, vol. 10, pp. 88152-88163, 2022, doi: 10.1109/ACCESS.2022.3199347.
- [37] A. S. B. Azam, A. A. Malek, A. S. Ramlee, N. D. S. M. Suhaimi, and N. Mohamed, "Segmentation of breast microcalcification using hybrid method of canny algorithm with otsu thresholding and 2D wavelet transform," in *Proceedings of the 2020 10th IEEE International Conference on Control System, Computing and Engineering (ICCSCCE)*, 2020, pp. 91-96, doi: 10.1109/ICCSCCE50387.2020.9204950.

BIOGRAPHIES OF AUTHORS






Akmal Shafiq Badarul Azam    received his B.Sc. in Computational Mathematics and M.Sc. in Applied Mathematics (Financial and Management Mathematics) from the Universiti Teknologi MARA (UiTM), Malaysia, in 2021 and 2022, respectively. He is currently pursuing a Ph.D. in Mathematics at UiTM. His research interests include mathematical image analysis, medical image processing, and machine learning. He can be contacted at email: akmalshafiq@uitm.edu.my.






Abdul Kadir Jumaat    received his B.Sc. and M.Sc. in Mathematics from the Universiti Teknologi MARA (UiTM) in Shah Alam, Malaysia, as well as his Ph.D. in Applied Mathematics (Mathematical Imaging Methods) from the University of Liverpool in the United Kingdom. He is currently employed by UiTM Shah Alam in Malaysia as a research fellow at the Institute for Big Data Analytics and Artificial Intelligence (IBDAAI) and a senior lecturer in the School of Mathematical Sciences, College of Computing, Informatics, and Mathematics. His research interests include image/signal processing, artificial intelligence, computer vision, biometrics, medical image and analysis, and pattern recognition. He can be contacted at email: abdulkadir@tmsk.uitm.edu.my.






Mohd Azdi Maasar    is presently employed as a senior lecturer in mathematics and a Collaborative Group Fellow in Big Data Analytics at the University Technology MARA. He earned his Bachelor of Science in Mathematics (Hons) from the same university before going on to earn his Master of Financial Mathematics from the University of Wollongong in Australia and his Master of Science (Research) in Mathematics from Brunel University in London. His research interests span a wide range of mathematical disciplines, including financial mathematics, risk management, and data analytics. He can be contacted at email: azdimaasar@tmsk.uitm.edu.my



Mohamed Faris Laham    received B.Sc. in Mathematics from the Universiti Teknologi MARA (UiTM) Shah Alam and M.Sc. in Mathematics from the Universiti Kebangsaan Malaysia. Universiti Putra Malaysia employs him as a Research Officer at the Institute for Mathematical Research (INSPERM). His research interests include computational mathematics and financial engineering. He can be contacted at the email address: mohdfaris@upm.edu.my.



Normahirah Nek Abd Rahman    obtained her B.Sc. in Mathematics (2011) and M.Sc. (Mathematics) from Universiti Kebangsaan Malaysia and Ph.D. in Mathematical Cryptography (2017) from Universiti Putra Malaysia. Her research area is mathematical cryptography, number theoretical cryptography and cryptanalysis, and public key cryptography. Currently, she is a Senior Lecturer at Universiti Kebangsaan Malaysia. She can be contacted at the email address: normahirah@ukm.edu.my.